JACS
JOURNAL OF THE AMERICAN CHEMICAL SOCIETY
Article
pubs.acs.org/JACS

The Fuzzy Quantum Proton in the Hydrogen Chloride Hydrates

Ali A. Hassanali,*[,†,‡] Jérôme Cuny,*[,†,‡] Michele Ceriotti,[§] Chris J. Pickard,[∥] and Michele Parrinello[†]

[†]Department of Chemistry and Applied Biosciences, ETH Zurich and Università della Svizzera Italiana, via G. Buffi 13, CH-6900 Lugano, Switzerland

[§]Physical and Theoretical Chemistry Laboratory, University of Oxford, South Parks Road, United Kingdom

[∥]Department of Physics and Astronomy, University College London, Gower Street, United Kingdom

Supporting Information

ABSTRACT: The motion of the excess proton is understood as a process involving interconversion between two limiting states, namely, the Eigen and Zundel cations. Nuclear quantum effects (NQE) and the organization of the surrounding solvent play a significant role in this process. However, little is known about how these factors can change the limiting state in molecular systems and the physicochemical properties of its surrounding hydrogen-bond environment. In this work we use state of the art ab initio molecular dynamics simulations to examine the role of NQE on the nature of the proton in four hydrogen chloride hydrates. We demonstrate that NQE significantly alter the phase space properties of the proton and that the local electronic structure of the proton is an exquisitely sensitive indicator of the limiting state in each of the crystals. We evaluate both the proton momentum distribution and the proton chemical shifts and demonstrate that deep inelastic neutron scattering and solid-state nuclear magnetic resonance experiments can serve as complementary techniques for probing the quantum nature of the proton in hydrogen-bonding systems. We believe that the rich and insightful information we obtain for these acid hydrates provides a motivation for new experimental studies.

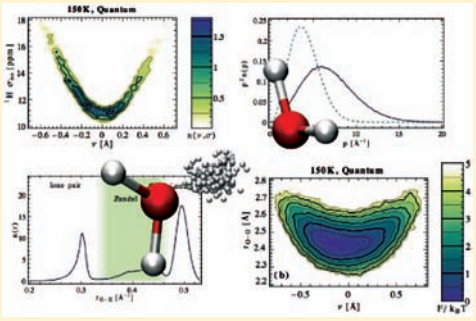

1. INTRODUCTION

Proton transfer (PT) plays a critical role in numerous chemical and biological processes.[1] These processes range from the simple acid−base chemistries that control the pH of water and the pK_a's of amino acids[2,3] to signaling transduction events in biological systems.[4] Most of the acid−base chemistry occurs in water in which excess protons move via structural diffusion in a process known as the Grotthuss mechanism.[5−11] This mechanism is understood in terms of the interconversion between the Eigen and the Zundel cations. The Eigen cation is composed of a central hydronium ion (H_3O^+) solvated by three water molecules ($H_9O_4^+$).[12] In contrast, in the Zundel cation ($H_5O_2^+$), the excess proton is shared between two water molecules.[13] Obviously, during a PT event the excess proton passes through a number of intermediary states between Eigen and Zundel. Despite the progress in this field, there is still some contention about both the structure of the dominant form of the proton in bulk water and the critical factors that control the relative proportion of Eigen, Zundel, and the continuum of intermediate states that lie in between them.[7−11,14−16] Theoretical studies have shown that nuclear quantum effects (NQE) have a significant effect on the limiting state of the proton in various hydrogen-bonded systems.[1,17−21] One can also imagine that asymmetries of the solvent environment surrounding the proton will have some influence on its properties. Quantifying the relative magnitudes of these effects is critical if we are ever to understand bulk water chemistry and protonated systems in general.

Unfortunately, the structure of the proton is challenging to characterize in bulk water in both experiments and theory.[7,10,14−16,22] This is mainly due to the fast time scale of PT and the complex role played by the surrounding solvent. One way of dissecting the molecular mechanisms of PT is to examine solid-state structures in which the excess proton lies in a more constrained environment.[23,24] This allows one to more easily isolate the relative roles of NQE and asymmetries on the limiting state of the proton. The pioneering work by the late Victoria Buch suggested that the hydrogen chloride hydrates (acid hydrates) could serve as excellent model systems for protonated water.[25,24] On the basis of the position of the heavy atoms, X-ray diffraction studies proposed the following chemical formulas for the four acid hydrates: ($H_3O^+Cl^-$) for the monohydrate,[26] ($H_5O_2^+Cl^-$) for the dihydrate,[27] ($H_5O_2^+Cl^-\cdot H_2O$) for the trihydrate,[28] and finally ($H_9O_4^+Cl^-\cdot 2H_2O$) for the hexahydrate.[29]

The goal of this work is to use theory to determine which are the most appropriate experimental tools for investigating the nature of the excess proton and the role of NQE in the hydrogen chloride hydrates. Hayes and co-workers recently reported an impressive study of the triflic acid hydrates using path integral (PI) simulations, which is the gold standard method for including NQE.[30,31] To circumvent the high computational cost of PI, we use the most recent theoretical

Received: February 14, 2012
Published: April 14, 2012

dx.doi.org/10.1021/ja3014727 | J. Am. Chem. Soc. 2012, 134, 8557−8569

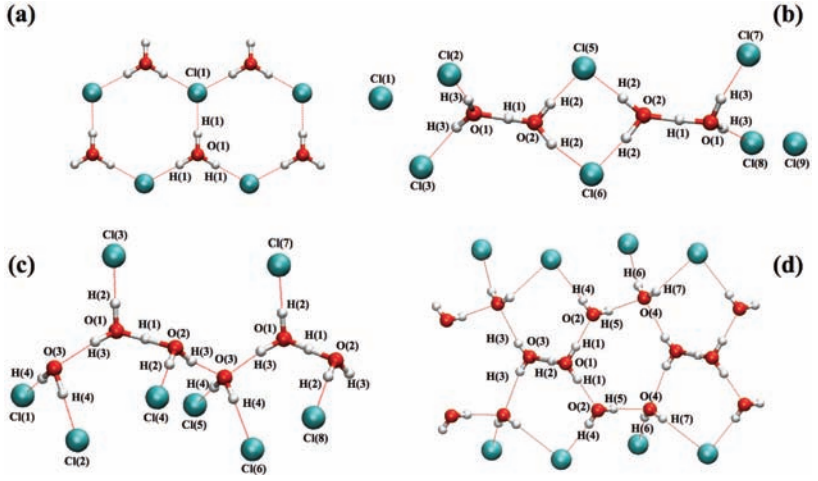

Figure 1. Representative unit structures forming the (a) monohydrate, (b) dihydrate, (c) trihydrate, and (d) hexahydrate. Labels are referred to in the text.

advances made in our group to include NQE using sophisticated thermostatting techniques in ab initio molecular dynamics simulations (AIMD).[32] We demonstrate that the structural properties of the excess proton in each acid hydrate is distinct and characterized by a significant fluxional behavior. We analyzed the proton momentum distributions ($n(p)$), which can be examined experimentally using deep inelastic neutron scattering (DINS) measurements.[33] Our results suggest that this technique provides a macroscopic probe of NQE on the kinetic energy (KE) of the system but is unable to distinguish between crystallographically distinct protons. In contrast, using recently developed theoretical tools, we have shown that probing protons in different hydrogen-bond (HB) environments should be possible by looking at their chemical shift (CSt) parameters with solid-state nuclear magnetic resonance (SSNMR), which has a greater sensitivity to small variations in the electronic structure.[34,35] Our studies should have important implications for establishing experimental probes that could be used to probe the role of NQE in a broad range of different hydrogen-bonded compounds.

Besides being model systems for studying the structural properties of protonated water, understanding the chemical make up of the hydrogen chloride hydrates has important implications in the area of atmospheric chemistry. It is well appreciated that depletion of the ozone layer is intrinsically tied to specific chemical processes that occur on the surface of ice that forms in polar stratospheric clouds.[36,37] Adsorption of HCl onto ice and the subsequent chemistry that leads to formation of chlorine is believed to be one of the essential processes involved in the extinction of the ozone layer.[36,37] It is thus critical to develop a molecular understanding of the solvation phenomena of HCl in water.

The paper is laid out as follows: we begin by describing the structures of the four acid hydrates and the computational methods used in section 2. In section 3 we characterize the influence of NQE on the structural properties of the proton and analyze the $n(p)$ of the four acid hydrates. In section 4 we report the analysis of the electronic structure and the NMR properties of the protons in these compounds. Finally, we end with some concluding remarks on our work in section 5.

2. COMPUTATIONAL METHODS AND STUDIED COMPOUNDS

2.1. Structures of the Compounds Studied. The structures that form the four hydrogen chloride hydrates that are examined in this work are shown in Figure 1, while the corresponding crystallographic data are summarized in Table 1.

Table 1. Experimental Crystallographic Data of the Four Acid Hydrates Determined by Single-Crystal X-ray Diffraction

compounds	a (Å)	b (Å)	c (Å)	β (deg)	Z
monohydrate[26] (rhombohedral)	4.05	4.05	4.05	73.50	1
dihydrate[27] (monoclinic)	3.991	12.055	6.698	100.58	4
trihydrate[28] (monoclinic)	7.584	10.154	6.715	122.96	4
hexahydrate[29] (orthorhombic)	6.3302	6.4528	17.8979	90.0	4

As shown in Figure 1a, the monohydrate is composed of H_3O^+ ions surrounded by three Cl^- ions that form a laminar arrangement of similarly oriented trigonal pyramids. Instead of being hydrogen bonded to three water molecules, the H_3O^+ ion is surrounded by three Cl^- ions. Because of this structural similarity, we will refer to this motif as an Eigen-like cation. The X-ray diffraction data suggests that the H_3O^+ occupies two positions with equal probability.[26] However, introducing this disorder only improves the R factor by 0.1%. As we will show later, this apparent disorder can be ascribed to the fluxional nature of the H_3O^+, which could not be captured using those early refinement techniques.[26] Furthermore, previous calculations of the monohydrate have also indicated that the disordered state is unstable.[24,38]

The X-ray crystallographic data for the di- and trihydrate indicate that some of the O−O distances between two water molecules (O(1)−O(2) in Figure 1b,c) are more compressed (~2.4 Å) compared to what one would expect in bulk water. These short bonds led the experimentalists to conclude that the proton is symmetrically shared between the water molecules forming a Zundel cation ($H_5O_2^+$).[27,28] In the trihydrate, the water molecules form chains in which the $H_5O_2^+$ species are bridged by one water molecule (O(3) in Figure 1c). This water molecule is linked to two $H_5O_2^+$ ions by two HB (the two O(3)−H(3) bonds in Figure 1c).

Finally, the crystallographic structure of the hexahydrate suggests that an H_3O^+ ion is surrounded by a solvent cage made up of water molecules and Cl^- ions.[29] The smallest O−O bond length in the

dx.doi.org/10.1021/ja3014727 | J. Am. Chem. Soc. 2012, 134, 8557−8569

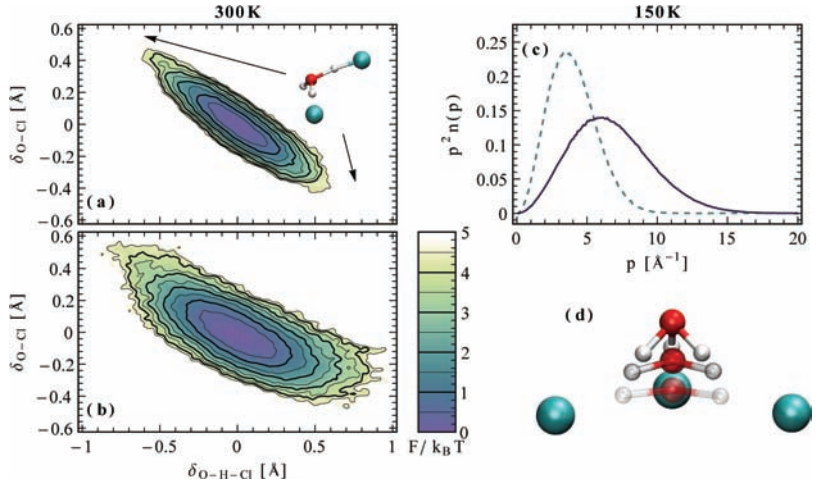

Figure 2. Distributions of δ_{O-H-Cl} and δ_{O-Cl} for simulations of the monohydrate at 300 K without (a) and with (b) NQE (see text for details). Representative snapshot of the Zundel-like state formed between a water and a Cl^- is also shown. (c) Radially averaged $n(p)$ for the monohydrate at 300 K with (black) and without (light, dashed) NQE. Quantum $n(p)$ differs from the classical Maxwell–Boltzmann distribution. (d) Schematic representation of the umbrella-breathing motion observed for the H_3O^+ ion.

hexahydrate is ~2.5 Å. The dominant limiting state of the proton in this compound was interpreted to be the Eigen cation ($H_9O_4^+$).

2.2. Computational Methods. AIMD simulations were performed using Quickstep, which is part of the CP2K package.[39] In these calculations, Born–Oppenheimer molecular dynamics is used for propagation of the nuclei. The electronic orbitals are converged to the Born–Oppenheimer surface at every step in the molecular dynamics simulation using extrapolation techniques borrowed from the Car–Parrinello method.[40] In our simulations, we will refer to quantum and classical simulations as simulations performed with and without NQE. A convergence criterion of 5×10^{-8} au was used for optimization of the wave function. Using the Gaussian and plane waves (GPW) method, the wave function was expanded in the Gaussian DZVP basis set while an auxiliary basis set of plane waves was used to expand the electron density up to a plane wave cutoff of 300 Ry. In these calculations the Brillouin zone is sampled at the Γ point. The core electrons are treated using the Goedecker–Teter–Hutter (GTH) pseudopotentials.[41] We used the Becke–Lee–Yang–Parr gradient correction[42,43] (BLYP) to the local density approximation. While the BLYP functional is known to overstructure water, it has been also shown to give a good description of both the structural and the dynamical properties of the excess proton and hydroxide ion in bulk water.[1] Furthermore, most of the structural properties we are interested in are dominated by the short-range electrostatics between the protonated species and the counterions (Cl^-), and hence, dispersion corrections are unlikely to change the qualitative picture presented in this work.

For all the acid hydrates, we conducted simulations at both 150 and 300 K in order to examine the role of finite temperature effects on the structural properties of the proton. For the monohydrate and dihydrate, we found that the experimental unit cells yielded spurious configurations, and hence, larger supercells were used to simulate these systems (see Supporting Information). All simulations were thermostatted using the framework of the generalized Langevin equation (GLE), which allows one to optimally sample vibrational modes spanning a broad range of frequencies.[32] This methodology provides a practical way of including NQE in classical simulations by selectively thermostatting different modes of the system at a temperature so as to mimic the role of zero-point energy.[32] The quantum simulations were performed using the quantum thermostat (QT). The NQE were investigated at both 150 and 300 K through a comparison of the results of classical simulations with those obtained using the QT. Time steps of 0.5 and 0.25 fs were used for the classical and quantum simulations, respectively (see Supporting Information for details of simulation lengths). An important goal of this work was to extract and compare the $n(p)$ for the various acid hydrates. The QT preserves the quantum fluctuations of the momenta,[44] and so, $n(p)$ can easily be obtained from these simulations. If one is only interested in the structural properties, it is also possible to systematically converge the NQE by combining the GLE with PI.[45] In order to assess the accuracy of the QT, we compared some of the structural properties of the monohydrate, obtained from the simulations with the QT, to those obtained using PI+GLE. This hybrid method indicates that for the structural properties considered here PI+GLE reaches convergence with fewer than four beads and that the QT significantly corrects the unphysical localization of the protons observed in the classical simulations (see Supporting Information). We decided to use the QT rather than the more accurate PI+GLE because only the former provides straightforward access to $n(p)$. At present, the only rigorous way of computing the momentum distribution involves performing full PI simulations and applying open path techniques, which are computationally demanding.[46]

The NMR chemical shielding (CSg) tensors were evaluated using the CASTEP density functional theory code which describes the extended structure of systems using periodic boundary conditions.[47] The core–valence interactions were described with the ultrasoft pseudopotentials (US-PP) generated using the OTF-ultrasoft pseudopotential generator included in CASTEP. The gauge-including projector augmented-wave (GIPAW) formalism was used to calculate CSg tensors from the pseudo-electronic density.[48,49] This approach has proven to be successful for examining structural and dynamical properties in a large range of solid-state materials.[50] For each atom, the three shielding parameters, σ_{iso}, σ_{aniso}, and η_σ, are calculated from the eigenvalues of the CSg tensor (σ_{xx},σ_{yy},σ_{zz}) using $\sigma_{iso} = (\sigma_{xx} + \sigma_{yy} + \sigma_{zz})/3$, $\sigma_{aniso} = \sigma_{zz} - \sigma_{iso}$, $\eta_\sigma = (\sigma_{yy} - \sigma_{xx})/\sigma_{aniso}$, with $|\sigma_{zz} - \sigma_{iso}| \geqslant |\sigma_{xx} - \sigma_{iso}| \geqslant |\sigma_{yy} - \sigma_{iso}|$.[51] In this work, we will refer to calculated chemical shielding values and not to chemical shift ones, as we were only interested in relative differences. The ^1H σ_{iso} values we obtained were converged with respect to our choice of 500 eV for the energy cutoff. We used a 2×2×2, 4×2×4, 4×4×4, and 4×4×2 Monkhorst–Pack k-point grid for the mono-, di-, tri-, and hexahydrate, respectively.[52] With these parameters the numerical error of the ^1H σ_{iso} values is less than 0.1 ppm. The time scale of the NMR measurements is several orders of magnitude longer than the characteristic frequencies of the probed systems. Hence, experiments can only probe an averaged chemical shift tensor for each crystallographically independent proton. To take this effect into account in the framework of AIMD, we followed the procedure proposed by Dumez et al.[53] For each independent proton, this consists of linearly averaging the matrix element of the CSg tensors expressed in a fixed Cartesian frame over an ensemble of configurations. The resulting averaged tensor is then diagonalized, which leads to the corresponding averaged shielding parameters ($\bar{\sigma}_{iso}$,

dx.doi.org/10.1021/ja3014727 | J. Am. Chem. Soc. 2012, 134, 8557–8569

$\overline{\sigma}_{aniso}$, $\overline{\eta}_{\sigma}$). The ensemble average was performed over 100, 200, 200, and 300 frames uniformly sampled from the simulations of the mono-, di-, tri-, and hexahydrate, respectively. The convergence of ensemble-averaged CSg parameters has been studied by several authors in organic crystals.[53−55] Although full convergence is hard to achieve, these studies have shown that meaningful results can be obtained by this approach. In the case of the monohydrate, the frames extracted from the simulations have been transformed from the rhombohedral to the hexagonal representation because it was difficult to obtain satisfactory convergence of the NMR parameters with the rhombohedral unit cell.

3. PROTON STRUCTURE AND ANALYSIS OF THE PROTON MOMENTUM DISTRIBUTIONS

We now present the effects of NQE on the structural properties of the proton in each of the acid hydrates. This analysis highlights the fluxional nature of the proton and its coupling to the surrounding environment. We also present an analysis of the challenges involved in interpreting the $n(p)$ from DINS experiments.

3.1. Monohydrate. The crystallographic structure of the monohydrate is relatively simple and symmetric (see Figure 1a). However, closer inspection of the crystal reveals new interesting features. For example, the hydronium ions point in the same crystallographic direction, so there is a net dipole moment in the unit cell, which suggests that this compound could be ferroelectric. The experimental unit cell likely forms one of many possible domains as stabilizing a net dipole moment would be energetically costly.[25,56] In our simulations, we found that the H_3O^+ undergoes an umbrella-breathing mode during which it fluctuates between a pyramidal and an almost planar geometry (see Figure 2d). Due to the global symmetry of the crystal, changes in the dipole moment of the system will be dominated by this fluxional character in the [111] crystallographic direction. We quantified this effect by determining the distance (z_u) between the oxygen atom of the H_3O^+ and the triangular plane formed by the three Cl^- surrounding it.[57] The fluctuations of z_u is in some sense a measure of the electrical susceptibility of the system. Our results indicate that both finite temperature and NQE have a significant effect on this quantity. For the 150 K simulations with and without the QT $z_u \approx 0.938$ (0.023) and 0.957 (0.016) Å, respectively, while for the 300 K simulations with and without the QT $z_u \approx 0.900$ (0.049) and 0.931 (0.041) Å, respectively. The numbers in parentheses refer to the fluctuations of z_u. These results suggest that the monohydrate could exhibit a phase transition in its dielectric properties as a function of temperature. Furthermore, this fluxional character provides some rationale for the suggested disorder in the position of the hydronium.[26]

NQE cause the proton to be more delocalized as seen in the radial distribution functions (see Supporting Information). The enhanced fluctuations that arise because of the NQE on the O−H and H−Cl bonds imply that there are PT events that lead to transient Zundel-like states where the proton is shared between a water molecule and Cl^- ($H_2O{-}H^+{-}Cl^-$). A representative snapshot of one of these events is shown in Figure 2a. This PT event involves compression of the heavy oxygen of the water and the Cl^-. In order to quantify this effect, we examined an order parameter defined by $\delta_X = r_{X,1} - ((r_{X,2} + r_{X,3})/2)$. X refers to either the distance between the hydronium oxygen and the Cl^- (r_{O-Cl}) or the symmetrized proton transfer coordinate along that O−Cl bond ($r_{O-H} - r_{H-Cl}$). The numbered subscripts i in $r_{X,i}$ refer to the three possible HB around the hydronium. Figure 2a,b shows the free energy surfaces along the order parameters δ_{O-H-Cl} and δ_{O-Cl} for the classical and quantum simulations at 300 K, respectively.[58] In these surfaces, the minimum in free energy is located at ∼(0,0) so the limiting state is an Eigen-like cation. However, when we compare the two surfaces shown in parts a and b in Figure 2, we observe that there is a tendency for the proton to delocalize between the O−Cl bonds during the quantum simulation. These effects are similar to the findings of recent X-ray absorption fine structure (XAFS) experiments on the structure of H_3O^+ and Cl^- in concentrated HCl where shared, proton-bridging structures are observed.[59] This effect has also been found in very recent full PI calculations of hydrated HCl clusters by Marx and co-workers.[60]Access to the momenta from the simulations with and without the QT allows us to conveniently compare the $n(p)$ of the protons from the classical and quantum simulations. The results show that the radially averaged proton momentum distribution ($p^2n(p)$) is significantly altered from the classical results (see Figure 2c). Inclusion of NQE alters the Gaussian character of the $n(p)$ due to the anisotropy of the potential that the protons experience along different crystallographic directions.[44] Furthermore, when NQE are incorporated the protons in the monohydrate exhibit enhanced KE (∼856 K) compared to the classical results (∼299 K). This is consistent with the presence of enhanced delocalization of the proton's position when NQE are included.

3.2. Dihydrate. The X-ray structure of the dihydrate suggests that the excess proton is tightly sandwiched between two water molecules to form an $H_5O_2^+$ species. These species are surrounded by an asymmetric solvent cage made up of Cl^- ions (see Figure 1b). The O−H $g(r)$ for the dihydrate is broader than the monohydrate because of the compressed O(1)−O(2) bond (see Supporting Information for $g(r)$ of the monohydrate). In Figure 3 we show a comparison of the O−H

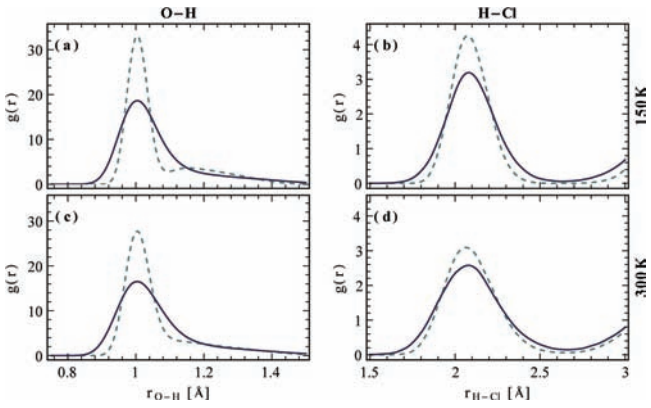

Figure 3. O−H pair correlation functions of classical (light, dashed line) and quantum (dark line) simulations at 150 (a) and 300 K (c) in the dihydrate. H−Cl pair correlation functions of classical (light, dashed line) and quantum (dark line) simulations at 150 (b) and 300 K (d).

$g(r)$ from the classical and quantum simulations of the dihydrate which demonstrates that NQE have a significant effect on the delocalization of the proton and that this effect is more pronounced in the lower temperature simulations, as expected. In particular, we observe that the classical simulations at 150 K reveal a small shoulder in the O−H $g(r)$ that develops due to the presence of the shared proton. This feature gets washed out when we include NQE. Although NQE increase the

dx.doi.org/10.1021/ja3014727 | J. Am. Chem. Soc. 2012, 134, 8557−8569

delocalization of the proton between H_2O and Cl^-, this effect is much less pronounced than in the monohydrate (see Figure 2) because the O−Cl bond in the dihydrate is less compressed. A common trick that has been used in the literature to account for the NQE in bulk water at ambient conditions is to perform simulations of the system at a higher temperature.[61,62] Simulations at elevated temperatures reduce the overstructuring of the O−O $g(r)$ that is often found in AIMD simulations.[61] The O−H $g(r)$ from the quantum simulation at 150 K is quite different from that in the classical simulation at 300 K. It is clear that temperature and NQE influence the short- and long-range parts of the $g(r)$ in different ways, and so, a uniform change of temperature cannot be used to mimic NQE. This is consistent with previous studies that compare the role of finite temperature and NQE on the structural and dynamical properties of bulk water using both empirical and ab initio based potentials.[63−65]

The classical and quantum $n(p)$ for all protons in the dihydrate differ significantly (see Supporting Information) as seen in the difference in the total KE of the protons from the classical and the quantum simulations (∼301 vs ∼894 K, respectively). The total $n(p)$ in the dihydrate is an average over two types of protons: those that are shared between the compressed O(1)−O(2) bond, and those that participate in H−Cl bonds. These protons experience different electrostatic environments which can effect the tails of the $n(p)$ distribution. In Figure 4a we show the radially averaged $n(p)$ for the two

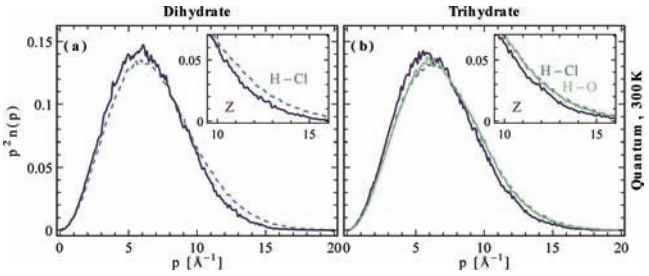

Figure 4. (a) Radially averaged $n(p)$ comparing the protons participating in H−Cl HB (light, dashed line) and those partially shared between the compressed O(1)−O(2) bond (dark line) in the dihydrate. (b) Radially averaged $n(p)$ comparing the protons participating in H−Cl HB (light, dashed line), those shared between the compressed O(1)−O(2) bond (dark line), and the protons of the Zundel that are hydrogen bonded to a water molecule (light line) in the trihydrate. Corresponding KE of these three types of protons are ∼943, ∼846, and ∼933 K, respectively, which reflects the relative strengths of the different HB. Insets show the tails in the $n(p)$. See text for further details.

types of protons that we extracted from the quantum simulations at 300 K. The shared protons exhibit a shorter tail in the radial $n(p)$, as would be expected for protons along more compressed bonds.[66] On the other hand, the protons that are hydrogen bonded to the Cl^- have a longer tail in the $n(p)$ which indicates that the proton is more strongly localized in configurational space. These features are also reflected in the difference between the average KE of the two types of protons (∼802 K for the shared proton vs ∼917 K for the protons in H−Cl bonds). These results are consistent with Heisenberg's uncertainty principle and further demonstrate that the QT performs quite well in capturing these essential physical properties. These results should help guide the interpretation of the experimentally measured $n(p)$ in these systems when they become available.

Having established the role of NQE on the configurational and momentum properties of the protons in the dihydrate we now give a more quantitative analysis of the role of these effects on the nature of the dominant limiting species (Eigen vs Zundel). Previous theoretical studies of the dihydrate by Buch et al. and Sillanpää et al. suggested that the proton tended to localize more toward one of the oxygens (O(1)).[24,67] Thus, instead of being a symmetrically shared proton, as suggested by the experimentalists, the proton in the dihydrate more closely resembled an Eigen-like state. However, these studies did not examine the origin of this symmetry breaking in the crystal. Furthermore, the effects of including NQE has not been the subject of previous theoretical studies of the acid hydrates.[24,67]

Our results indicate that the average position of the proton along the O(1)−O(2) bond arises through a delicate balance between NQE and the local electrostatic potential. As shown in Figure 1b, one of the water molecules (O(2)) in the dihydrate is hydrogen bonded to two Cl^- ions that is thus part of a square-like ring structure (O(2)−Cl(5)−O(2)−Cl(6)). This structural motif is not observed for the other water molecule in the structure—the one that forms part of the shared proton complex. This difference in the local structural environment of each water molecule implies that there is a higher density of Cl^- near one of the water molecules (O(1) in Figure 1b). Consequently, there is an asymmetric electrostatic potential on the shared proton and hence a tendency for it to localize away from the square-like ring and form a species that more closely resembles a distorted Zundel-like state. These effects are quantified in Figure 5, which shows the free energy surface as a

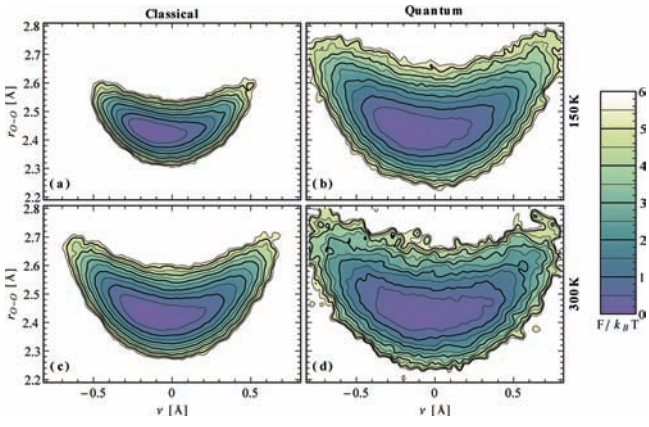

Figure 5. Coupling of the compression of the O(1)−O(2) bond and symmetrized PT coordinate (ν) in the dihydrate for simulations at 150 and 300 K with and without NQE.

function of the distance between the heavy oxygen atoms (O(1)−O(2)) and the canonical symmetrized proton transfer coordinate ($\nu = r_{O(1)-H(1)} - r_{H(1)-O(2)}$). In both the classical and the quantum simulations at 150 and 300 K we observe that there is a marked tendency for the proton to localize on one side of the distribution. Figure 5a,b shows that this feature is more prominent in the lower temperature simulations. NQE tend to soften the overall potential, resulting in more enhanced fluctuations of the proton which enhance the transient formation of Zundel-like states. However, the dominant state in all simulations of the dihydrate resembles a distorted Zundel-like cation rather than the idealized Zundel cation. Although

dx.doi.org/10.1021/ja3014727 | J. Am. Chem. Soc. 2012, 134, 8557−8569

there is some tendency for the proton to localize on one water molecule, it does not form an Eigen-like state as previously suggested.[24,67]

It is well established that the motion of the proton in bulk water is characterized by a collective reorganization of the surrounding water molecules.[1,15,22] The acid hydrates provide excellent model systems for examining how PT along the O(1)−O(2) bond is coupled to the vibrations of the surrounding lattice structure, without having to deal with the complexity of the rapidly evolving solvent environment. We took advantage of the asymmetry surrounding the solvated proton to examine the nature of the coupling of the PT coordinate (ν) to the relaxation of the surrounding environment using an order parameter defined by $r_{asym} = (r_{O(1)-Cl(2)} + r_{O(1)-Cl(3)}) - (r_{O(2)-Cl(5)} + r_{O(2)-Cl(6)})$ (see Figure 1c for details).[24] Figure 6 confirms that the motion of the proton

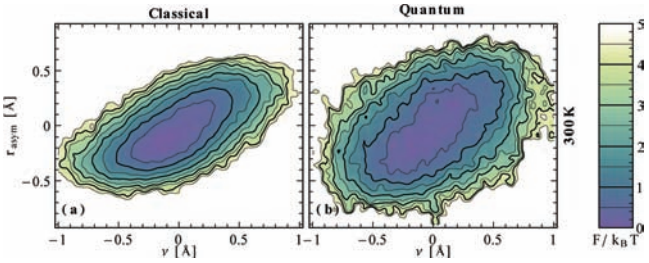

Figure 6. Coupling of the PT coordinate (ν) with vibrations of the surrounding Cl^- ion cage at 300 K without (a) and with (b) NQE.

along the O(1)−O(2) bond is coupled to strengthening or weakening of the HB with the surrounding Cl^- ions. As the proton shuttles across the compressed O(1)−O(2) bond and localizes on a single water, stronger HB to the Cl^- that are in close proximity to the proton develop, as one would qualitatively predict based on a simple Born solvation model. This is an example of reverse electrostriction[68,69]—the fluxional nature of the proton causes an increase in the local charge density which results in a compressive mode of the proton toward the Cl^-. Figure 6 shows that NQE have a significant effect on this process as they enhance delocalization of the proton toward the water molecule that is closer to the square ring. NQE thus has an indirect effect in increasing the strength of the HB in this part of the Cl^- cage.

The rattling of the proton between the two water molecules in the dihydrate and its coupling to the relaxation of the order parameter r_{asym} is reminiscent of the special-pair dance that is reported to occur for PT in bulk water.[5,6,15] In bulk water, a PT event is coupled to the loss of a HB being donated to the incipient H_3O^+.[5,6,15] However, in the dihydrate the waters sharing the proton do not have any HB being donated to the waters, and thus, the proton is able to freely shuttle back and forth transiently forming the Zundel states, followed by successful PT events forming the Eigen-like states.

3.3. Trihydrate. The structure of the trihydrate is similar to that of the dihydrate as it contains $H_5O_2^+$ cations. However, unlike the dihydrate, the $H_5O_2^+$ are linked together by a water molecule (O(3) in Figure 1c). From the total KE (~299 vs ~926 K) it is clear that there are marked differences in the quantum and classical $n(p)$ distributions for this compound. Figure 4b shows the separate contributions to the $n(p)$ that come from the protons in the three different HB environments (H(1), H(3), and H(2)/H(4)). Our results show that the protons shared between two water molecules exhibit a less enhanced tail at higher proton momentum values. Similarly to the dihydrate, the KE of the protons in different environments reflect the strength of the corresponding HB (see caption of Figure 4b). Interestingly, Figure 4b shows that the $n(p)$ distributions for the protons hydrogen bonded to Cl^- and for protons hydrogen bonded to water molecules along the water wires are indistinguishable.

Unlike the dihydrate, the excess proton in the trihydrate does not show a tendency to localize on one water molecule. To assess the extent to which the proton is shared in the trihydrate, we examined the coupling of the PT coordinate (ν) to the degree of compression of the oxygen atoms. Figure 7 shows

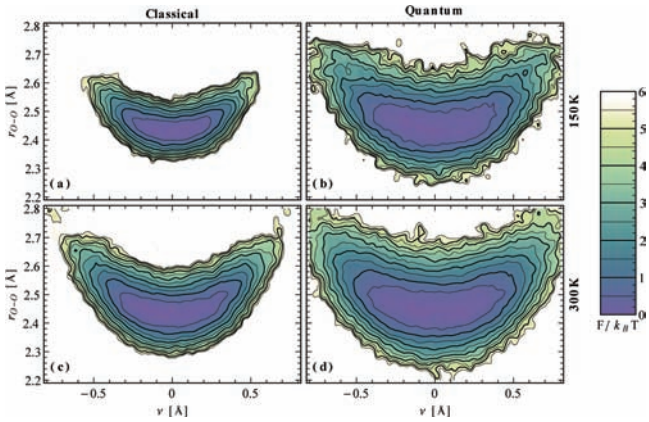

Figure 7. Coupling of the heavy atom compression of the O(1)−O(2) bond and symmetrized PT coordinate (ν) in the trihydrate for simulations at 150 and 300 K with and without NQE.

that in the classical simulations at 150 K the proton tends to be symmetrically placed at the center of the O(1)−O(2) bond. This is because the crystallographic environment around the proton in the trihydrate is more symmetric. Inclusion of NQE at both 150 and 300 K increases the delocalization of the proton, resulting in a much broader symmetric basin in the free energy surface plotted as a function of the PT coordinate. NQE thus enhance the transient formation of Eigen-like species while maintaining the average limiting Zundel state.

The trihydrate provides an interesting model system for examining how longer range lattice vibrations are coupled to the motion of the protons.[71] Beyond the rattling of the immediate solvent cage, we also find that there is a longer range coupling between the motion of protons in two Zundels that are bridged by a water molecule (for example, as seen in Figure 1c the two H(1) protons are separated by a HB wire along O(2)−O(3) and O(3)−O(1)). We examined the coupling between the PT coordinates of two water-bridged Zundel protons (ν_1 and ν_2). A coupling of these vibrational modes would suggest that there should exist correlations in the motion of the protons belonging to different Zundels in the crystal. Figure 8 illustrates that there is a strong coupling between the motions of the protons linked by the HB wire and that this feature is prevalent in both the classical and the quantum simulations. These correlations are absent in the dihydrate. It would be interesting to probe this feature experimentally.

3.4. Hexahydrate. The excess proton in the hexahydrate closely resembles the Eigen cation that is found in the monohydrate, except that it is immediately solvated by three water molecules rather than three Cl^- ions. Due to the presence

dx.doi.org/10.1021/ja3014727 | J. Am. Chem. Soc. 2012, 134, 8557−8569

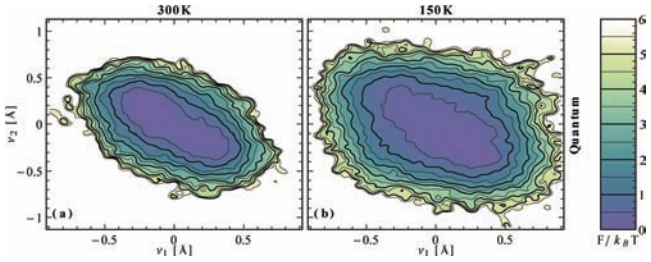

Figure 8. Correlation between the symmetrized PT coordinate for Zundels that are linked together by HB wires for the classical simulation (a) and quantum simulation (b) at 300 K of the trihydrate. Spearman's ranked correlation coefficient[70] ρ between the symmetrized PT coordinates is nonzero, which shows that the PT coordinates are significantly correlated (300 K classical $\rho = -0.53$, 300 K quantum $\rho = -0.34$, 150 K classical $\rho = -0.60$, 150 K quantum $\rho = -0.40$).

of a large hydration shell, we expected that longer range PT to nearby waters beyond rattling events might occur.[15] However, our simulations show that the excess proton is localized on a single water molecule (O(1) in Figure 1d). This result is consistent with recent work by Hayes and co-workers on triflic acid hydrates.[30,31] Unlike the di- and trihydrate, the crystal packing does not result in any significantly compressed O−O bonds. NQE tend to delocalize the proton and increase the excursions toward Zundel-like states, but on average, the limiting state is predominantly the Eigen cation.

In Figure 9a we focus on the $n(p)$ of the protons involved in the various HB that are present in the hexahydrate: the three

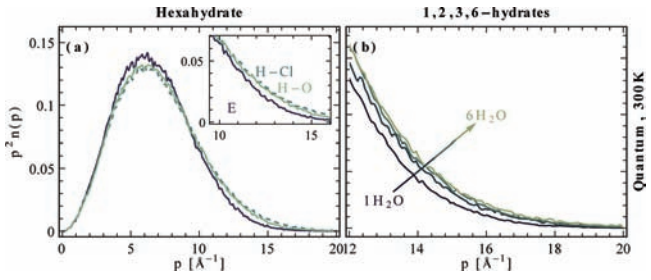

Figure 9. (a) Radially averaged $n(p)$ comparing the protons participating in H−Cl HB (light, dashed line), those forming the Eigen cation (dark line), and finally the protons hydrogen bonded to a water molecule (light line) in the hexahydrate. Total KE of the protons with and without NQE extracted from our simulations is ∼938 and ∼299 K, respectively. Corresponding KEs of these three types of protons are ∼978, ∼854, and ∼940 K. Insets show a blow up of the tails in the $n(p)$. (b) Blow up of the tails of the radially averaged $n(p)$ comparing the mono-, di-, tri-, and hexahydrate.

protons that form the Eigen cation (H(1) and H(2)), the protons that are hydrogen bonded to water molecules (H(3) and H(5)), and the protons that are hydrogen bonded to Cl^- ions (H(4), H(6), and H(7)). The data shows that the protons in the Eigen cation exhibit a less pronounced tail in the $n(p)$ similar to the protons shared between two water molecules in the di- and trihydrate. This demonstrates further that interpreting the $n(p)$ in terms of specific limiting states is not straightforward.

Two of the water molecules solvating the central H_3O^+ are hydrogen bonded to one Cl^- and one water molecule (O(2) in Figure 1d), while the third one donates a hydrogen bond to two water molecules (O(3) in Figure 1d). This results in an asymmetry in the surrounding proton environment. In order to quantify the extent to which the proton is delocalized in the hexahydrate we took advantage of this asymmetry and examined an order parameter $\delta_X = r_{X,1} - ((r_{X,2} + r_{X,3})/2)$, where X refers to either the distance between the hydronium oxygen and the waters immediately hydrogen bonded to it (d_{O-O}) or the symmetrized proton transfer coordinate along that O−O bond ($r_{O-H} - r_{H-O}$). The numbered subscripts i in $r_{X,i}$ refer to the three possible HB around the Eigen cation (the subscript 1 refers to the oxygen O(3) in Figure 1d). Figure 10

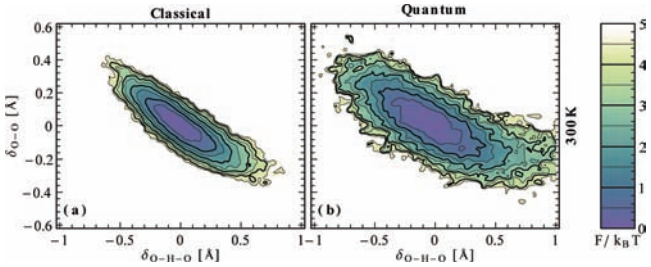

Figure 10. Distribution of δ_{O-H-O} and δ_{O-O} for simulations at 300 K without (a) and with (b) NQE in the hexahydrate.

shows the free energy surfaces along the order parameters δ_{O-H-O} and δ_{O-O}. Figure 10a shows that on average all three protons in the classical simulations are localized on the central oxygen, so the ion is an Eigen cation. However, there is a significant transient formation of Zundel-like states to all the neighboring water molecules as the proton performs the special-pair dance.[5,6,15] Figure 10b illustrates the effects of NQE on the distribution. Interestingly, we find that NQE significantly enhance the delocalization of the proton but that it still retains significant Eigen character. In fact, we find some tendency for the H(2) proton to be slightly more delocalized toward O(3) than H(1) toward O(2). The hexahydrate represents a limiting state of the proton that is somewhat intermediate between the classical localized Eigen-like cation of the monohydrate and the distorted Zundel cation in the dihydrate.

3.5. Synopsis. Having discussed the features of the proton momentum distribution for the four acid hydrates we can now compare their total $n(p)$ (see Figure 9b). There is a significant difference between the tail of the $n(p)$ for the monohydrate and the tails of the distributions in the other structures. The separation of the monohydrate from the rest results from a combination of compressed O−Cl bonds and only one type of HB in the crystal. Within the statistical uncertainties of our simulation we cannot quantitatively pin down differences in the $n(p)$ for the di-, tri-, and hexahydrate. However, Figure 9b suggests a qualitative trend where the tail of the distribution is slightly more enhanced as one moves from the di- to the hexahydrate. This is not surprising given that the presence of more water molecules results in a dominant signal from protons participating in normal HB which will exhibit longer tails in the radially averaged $n(p)$. It would be interesting to search for these features when the experimental $n(p)$ for these systems become available. The results for the $n(p)$ of all acid hydrates reported in this work shows that while this property serves as a clear marker for the presence of NQE, interpreting the structural origin of differences in the $n(p)$ in heterogeneous systems is quite challenging.

dx.doi.org/10.1021/ja3014727 | J. Am. Chem. Soc. 2012, 134, 8557−8569

4. PROTON ELECTRONIC STRUCTURE

The preceding analysis has shown that the acid hydrates provide excellent model systems for examining the spectrum of protonic states between the limiting Eigen and Zundel cations. The limiting state is controlled by an interplay between various factors including the intrinsic crystal packing which changes the spacing between the heavy atoms sharing the proton, finite temperature effects, NQE, and asymmetries in the local electrostatic potential. Although DINS experiments provide access to the role of NQE on the kinetic energy of the protons, inferring specific structural properties from the $n(p)$ is not straightforward because of the averaging over all the different chemical environments. Clearly, more sensitive experimental probes need to be used to probe the spectrum of proton states in the acid hydrates.

Previous work in our group has shown that subtle but sizable changes occur in the electronic environment of the proton during recombination of hydronium and hydroxide ions in water.[10] The electronic structure can be probed by examining the Wannier centers in the vicinity of the proton in each of the crystals. The Wannier centers provide a chemically intuitive way of characterizing the bonding properties in molecules.[72] A water molecule, for example, is characterized by two lone pair Wannier centers involved in hydrogen-bonding interactions and two bonding pair centers that are involved in covalent bonds.

4.1. Wannier Centers. For each of the hydrates, we identified the number of Wannier centers within 0.6 Å of the oxygen atom(s) on which the excess proton(s) resided. These distributions show that the electronic structure of the proton in each crystal is very different. Figure 11b shows the distribution of the Wannier centers for the proton in the mono- and hexahydrate. The proton in these crystals is in a state that is closer to the classical Eigen cation compared to what is observed in the di- and trihydrate. One thus obtains three bonding centers and one lone pair Wannier center. The peak associated with the bonding centers for the hexahydrate has a longer tail extending toward shorter distances compared to the monohydrate. This confirms the presence of the weak delocalization of the proton toward the surrounding solvating waters (section 3.4). Similar features have also been observed by Schwegler et al., who analyzed the distribution of Wannier centers for water undergoing dissociation under high-pressure conditions.[73] However, this analysis did not focus on using the Wannier centers to isolate the Eigen and Zundel cations. Figure 11a shows the same distributions for the di- and trihydrate, both of which are characterized by a "shared" proton that is the distorted Zundel-like cation and idealized Zundel limiting states, respectively. There is a striking difference in the Wannier center distributions shown in panels a and b in Figure 11. Both the di- and the trihydrate are characterized by a broad shoulder between 0.35 and 0.45 Å, which is absent for the mono- and hexahydrate. The shoulder appears because the lone pair Wannier centers of each water sharing the proton are engaged in a push−pull effect.[10] This process involves concerted but directionally opposite displacements of these lone pair Wannier centers during the PT process. This feature is striking and provides a new and unique way of identifying Zundel-like traits in the structure of the proton. The position of the lone pair Wannier center for the mono-, di-, and hexahydrate are very similar—they are all at 0.30 Å. However, for the trihydrate we observe a displaced lone pair peak position at 0.33 Å and a shoulder at 0.30 Å. One of the lone pairs accepts a weak HB from a water, while the other lone pair faces the lone pair of a water molecule in the crystal. This creates an asymmetry in the electrostatic potential experienced by the two lone pairs.

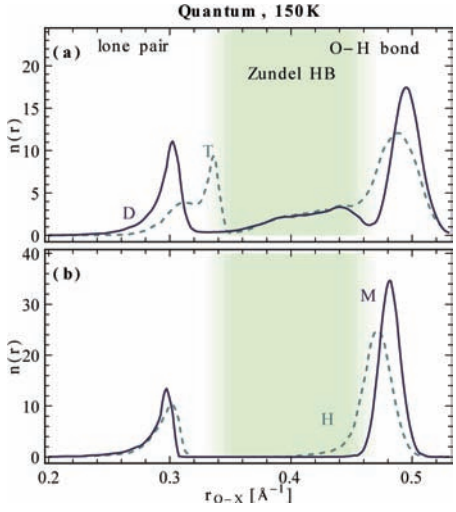

Figure 11. (a) Distribution of the positions of the Wannier centers with respect to the oxygen atom that forms the Eigen cation in the monohydrate and hexahydrate. (b) Same distributions for the shared proton in the dihydrate and trihydrate. These distributions were obtained from the simulations at 150 K using the QT.

This analysis suggests that an experimental probe sensitive to small variations in the electronic structure around a given proton is likely to serve as an effective probe of the proton's limiting state. The sensitivity of the ^{1}H chemical shift to the electronic structure suggests that it would allow for an unambiguous assignment of a particular resonance frequency with a specific proton electronic environment. We next turn to our analysis of the NMR chemical shifts for the protons in the different acid hydrates.

4.2. NMR Chemical Shifts. In the past decade, a number of experimental NMR studies have been complemented by quantum mechanical calculations.[74] In condensed matter systems, this has been achieved by use of periodic approaches[48,75−77] that have been applied to a number of chemical systems.[50,78−83] Very few of these studies have combined the calculation of NMR parameters with AIMD simulations to take into account the role of dynamical effects and ensemble averaging. Among these, we note previous work by Sebastiani and co-workers, who studied the ^{1}H isotropic CSt of liquid water and aqueous HCl.[81,84,85] In addition, a detailed analysis of the influence of dynamical effects on the ^{1}H and ^{13}C CSt parameters of organic solids has been provided by Dumez et al. and subsequent studies by other workers.[53−55] In contrast to molecular systems,[86−88] the influence of NQE on NMR properties has not been given much attention in condensed matter systems. Apart from the study by Dumez et al., who use a quasi-harmonic approximation to include zero-point energy effects,[53] the only reported study using PI and AIMD is by Ludueña et al.,[82] who examined the role of NQE in both lithium imide and amide. This study suggested a possible relationship between the isotropic chemical shift of protons and the corresponding HB lengths. However, interpreting and rationalizing the molecular origins of the observed changes induced by NQE remains a challenge in these materials. We now present a unique analysis of the NMR properties of the

dx.doi.org/10.1021/ja3014727 | J. Am. Chem. Soc. 2012, 134, 8557−8569

four acid hydrates. In the following, for brevity, we will focus our discussion on the isotropic chemical shielding parameter. For the interested reader, we show the same analysis for the chemical shielding anisotropy ($\overline{\sigma}_{aniso}$) and asymmetry ($\overline{\eta}_{\sigma}$) in the Supporting Information.

Monohydrate. We examined the role of finite temperature and NQE on the monohydrate by evaluating the ^{1}H CSg tensors from a set of configurations that were extracted from our AIMD simulations. Figure 12a illustrates the histograms of

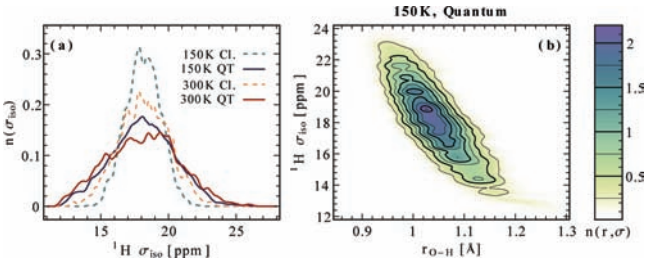

Figure 12. (a) Distribution of σ_{iso} calculated from the classical and quantum simulations at both 150 and 300 K for the monohydrate. Corresponding $\overline{\sigma}_{iso}$ values are presented in Table 2. (b) Distribution of σ_{iso} versus the corresponding O−H distances for the quantum simulation at 150 K.

the calculated σ_{iso} obtained from classical and quantum simulations at both 150 and 300 K. Each of these peaks corresponds to a unique average $\overline{\sigma}_{iso}$ value that is tabulated in Table 2. The data shows that inclusion of NQE or the increase of temperature increases the σ_{iso} fluctuations but does not alter $\overline{\sigma}_{iso}$. The origin of this effect comes from the ellipsoidal symmetry of the distribution of the ^{1}H σ_{iso} versus the O−H distances, which is shown in Figure 12b for the quantum simulation at 150 K. As the center and symmetry of this distribution is conserved over all simulations, $\overline{\sigma}_{iso}$ is not modified. It is also interesting to note that for larger fluctuations of the O−H bond, i.e., these corresponding to the delocalized Zundel-like species (see Figure 2a), the ^{1}H σ_{iso} distribution indicates some tendency to flatten. Because this effect involves rare fluctuations, it does not alter the symmetry of the distribution. It is likely that this feature will be more prominent in full PI simulations but will not change the overall physical picture presented.

Dihydrate. Figure 13b shows the σ_{iso} distribution obtained from the quantum simulation of the dihydrate at 150 K. This

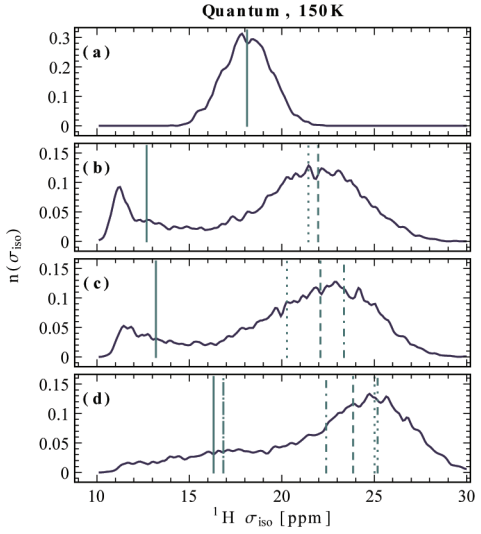

Figure 13. Distribution of σ_{iso} for the quantum simulations at 150 K for the mono- (a), di- (b), tri- (c), and hexahydrate (d). Lines highlight the positions of the $\overline{\sigma}_{iso}$ values found in Table 2. For the hexahydrate, H(6) and H(7) are represented by the same line (dashed double dotted).

distribution clearly shows that there are two distinct peaks that correspond to the two types of protons in the structure. The peak from the shared proton (H(1) in Figure 1b) is at low σ_{iso} values (solid line in Figure 13b). The peak at high σ_{iso} encompass all protons in H−Cl hydrogen bonds. This peak can be further divided into two subgroups: those belonging to the square rings (atoms H(2) in Figure 1b and represented by a dashed line), and those closer to the cluster of chloride ions (atoms H(3) in Figure 1b and represented by a dotted line). As can be seen in Table 2, these two subgroups of H−Cl protons exhibit different $\overline{\sigma}_{iso}$ values, which shows the asymmetry of the chemical environment around the distorted Zundel-like cation. In all our simulations (see Table 2) the difference in $\overline{\sigma}_{iso}$ values between the protons involved in H−Cl bonds and the shared protons is larger than ∼10 ppm. This difference is quite significant compared to the CSt range of protons in solid-state

Table 2. Averaged Isotropic Chemical Shielding ($\overline{\sigma}_{iso}$) Values Calculated from the Classical and Quantum Simulations at Both 150 and 300 K[a]

	monohydrate	dihydrate			trihydrate			
	H(1)	H(1)	H(2)	H(3)	H(1)	H(2)	H(3)	H(4)
150 K classical	18.14	11.74	22.10	21.40	12.62	22.05	20.22	23.62
150 K quantum	18.12	12.69	21.97	21.44	13.19	22.09	20.28	23.36
300 K classical	18.11	12.16	22.02	21.56	13.26	21.97	20.30	23.30
300 K quantum	18.09	12.83	21.75	21.39	13.53	22.02	20.35	23.40
	hexahydrate							
	H(1)	H(2)	H(3)	H(4)	H(5)	H(6)	H(7)	
150 K classical	16.23	15.91	23.57	25.08	22.14	25.21	25.26	
150 K quantum	16.31	16.84	23.86	25.02	22.40	25.18	25.20	
300 K classical	16.34	16.28	23.77	25.04	22.39	25.28	25.25	
300 K quantum	16.42	16.81	23.74	24.83	22.16	25.97	25.96	

[a]The errors on these values were evaluated by a block analysis and are lower or equal to 0.20 ppm in all cases. All values are in ppm. The numbering of the atoms is the same as in Figure 1.

dx.doi.org/10.1021/ja3014727 | J. Am. Chem. Soc. 2012, 134, 8557−8569

materials and is consistent with previous analysis of the $n(p)$ (see Figure 4).[35] This suggests the possibility to resolve these two types of protons experimentally. A comparison between panels a and b in Figure 13 reveals that the $\overline{\sigma}_{iso}$ value of the monohydrate lies in between the two main signals of the dihydrate. As already discussed, the H−Cl HB in the monohydrate is stronger than those in the dihydrate but weaker than the shared proton HB. Thus, the $\overline{\sigma}_{iso}$ of each proton provides a powerful way of discerning between weak and strong HB.

Closer inspection of the influence of temperature and NQE on the spectra reveals some interesting features. Both increasing the temperature and including NQE results in a broadening of the σ_{iso} distribution for all kinds of protons. Similar to the monohydrate, no significant variation in the average value of the H−Cl protons is observed (see Table 2). On the other hand, the behavior of the shared protons is significantly different as its $\overline{\sigma}_{iso}$ is shifted by ∼0.6−1.0 ppm. This particular behavior is directly related to the difference in the chemical environment of these two kinds of protons. We observe in Figure 14 that the lowest CSg values for the compressed proton

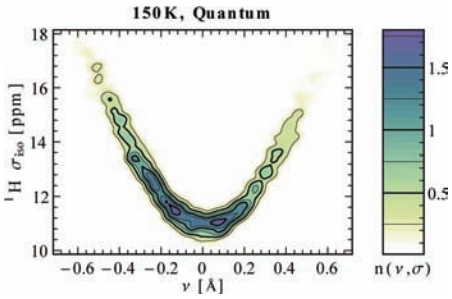

Figure 14. Distribution of σ_{iso} of the shared proton of the dihydrate along the PT coordinate (ν) for the quantum simulation at 150 K.

are obtained at the center of the O(1)−O(2) bond. Consequently, any increase in the fluctuations about this central position will populate higher σ_{iso} states, leading to an increase of $\overline{\sigma}_{iso}$. In the case of the dihydrate, although the equilibrium position of the proton is shifted from the center of the O(1)−O(2) bond, the population of the high σ_{iso} states (that correspond to short O−H bond lengths) is also sufficient to observe an increase of $\overline{\sigma}_{iso}$. Limbach et al.[88] recently rationalized the evolution for the ^{1}H isotropic chemical shift of the proton in an idealized $H_5O_2^+$ ion along various geometrical parameters. Consistent with our results, they obtain a correlation that is similar to that observed in Figure 14. This suggests that the trends shown for the σ_{iso} values could be a generic property for protons in compressed environments. However, in their study, NQE are incorporated in an empirical manner and do not result in any significant effect on the proton isotropic chemical shift. This is in sharp contrast with our results and likely due to the more rigorous inclusion of NQE and finite temperature effects in our simulations.

Trihydrate. The σ_{iso} distributions for the trihydrate exhibit similar trends to those seen for the dihydrate. These features are shown Figure 13c for the quantum simulation at 150 K. The low σ_{iso} values correspond to the signal from the Zundel protons shared between two oxygens (solid line on Figure 13c), and those at higher σ_{iso} values correspond to a mixture of three different protons, namely, the H−Cl hydrogen-bonded protons of the Zundel ion (dashed line on Figure 13c), the H−O hydrogen-bonded protons of the Zundel ion (dotted line on Figure 13c), and finally the protons of the free water molecules (dotted dashed line on Figure 13c). Each of these three types of protons corresponds to a different $\overline{\sigma}_{iso}$ value (see Table 2). In all our simulations, they are spaced by more than 1 ppm, which suggests that they should be experimentally resolvable. Compared to the dihydrate, the higher σ_{iso} peak in the trihydrate exhibits a broader distribution toward both higher and lower σ_{iso} values. This is due to the protons of the free water molecules (H(4)) and the H−O hydrogen-bonded protons of the Zundel ion (H(3)) that are absent in the dihydrate. The influence of finite temperature and NQE is similar to that in the dihydrate. The three kinds of protons at high $\overline{\sigma}_{iso}$ exhibit variations that are smaller than 0.3 ppm, whereas the influence on the Zundel proton is stronger. This effect is slightly less pronounced compared to the shared proton in the dihydrate because the proton in the trihydrate represents an idealized Zundel state, whereas in the dihydrate it is slightly more localized on one water molecule forming the distorted Zundel-like cation.

Hexahydrate. Finally, we examined the ^{1}H NMR properties of the hexahydrate. The distribution of σ_{iso} obtained from the quantum simulation at 150 K is shown in Figure 13d and shows two dominant regions. The high σ_{iso} values consist of a mixture of five different protons (H(3), H(4), H(5), H(6), and H(7) in Figure 1d corresponding to the dashed, dotted dashed, dotted, and dashed double dotted lines, respectively, on Figure 13d). The longer tail σ_{iso} region consists of the two protons forming the Eigen cation (H(1) and H(2) in Figure 1d corresponding to the solid and long dashed dotted lines, respectively, in Figure 13d). Table 2 shows that in all simulations the $\overline{\sigma}_{iso}$ values of H(1) and H(2) are close to each other and similar to those in the monohydrate. This confirms the Eigen character of the excess proton in the mono- and hexahydrate. Overall, the influence of temperature and NQE appears to be negligible on all protons but H(2). In this case, a weak sensitivity to NQE is observed which is consistent with our previous observations of section 3.4.

Synopsis. Previous studies examining the HCl acid hydrates and more recently the triflic acid family have focused on examining the IR spectra of different vibrational modes in the system.[24,30,31] Interpreting the IR spectra from these classical calculations in terms of specific structural and electronic properties of the proton is challenging and likely to be further complicated with inclusion of NQE. On the other hand, our results for the four acid hydrates demonstrate that ^{1}H SSNMR can characterize the limiting state of the proton, i.e., discriminate between the Zundel cation, the Eigen cation, and the intermediate states. Furthermore, NQE and finite temperature effects can have a resolvable influence on the CSt parameters, particularly for the di- and trihydrate.

5. CONCLUDING REMARKS

In this work, we examined the role of finite temperature and NQE on the structural properties of the hydrogen chloride hydrates. We thereby established some of the critical ingredients controlling the stability of the Eigen and Zundel cations and the continuum of states that are spread in between them. The structural landscape of the proton involves a coupling of several factors such as the role of asymmetries in the surrounding solvent environment, the extent of compression of the heavy oxygen atoms caused by crystal packing, and, of course, nuclear quantum effects.

dx.doi.org/10.1021/ja3014727 | J. Am. Chem. Soc. 2012, 134, 8557−8569

Overall, in the four hydrates we studied we find that the proton can exist as either the Eigen or the Zundel species. NQE cause an enhanced delocalization of the proton in all environments, but this does not appear to change the limiting state of the proton. Using PI simulations, Hayes and co-workers find similar features in the di-, tri-, tetra-, and pentahydrate of triflic acid.[30,31] The coupling of both the local asymmetries and NQE often results in somewhat unexpected physics. In the monohydrate, we find some tendency for the proton to be delocalized between the Cl^- and the water molecule that forms a transient Zundel-like state. This behavior has also been observed in the triflic acid dihydrate, where NQE result in spontaneous formation of SO_3H groups.[30] In the HCl dihydrate, the proton sits along a compressed hydrogen bond and NQE do not suppress the bias toward a distorted Zundel cation that is caused by asymmetries in the electrostatic potential. In the triflic acid hydrates, the sulfonate groups play a similar role as the Cl^- ions in the HCl hydrates by inducing asymmetries in the underlying electrostatic potential and hence in the position of the excess proton.[30,31] These results now provide a clearer picture of the fuzziness in the location of the protons, which was not resolvable in the original X-ray crystallography experiments.[26−29]

Previous theoretical studies of the excess proton in bulk water have suggested a higher probability of finding the Eigen-like species.[15,18] Our results suggest that one of the physical origins of this effect is the structural and electronic asymmetries around the proton caused by the surrounding solvent. In bulk water this asymmetry is reflected in the difference of the short-range behavior of $g(r)$ between the two waters sharing the proton.[15,18] Simons et al. have also shown that the heterogenity of bulk solvent induces significant asymmetry in the electron density around the central cation.[89] Another interesting aspect of the PT process in bulk water involves the notion of presolvation, where the surrounding solvent environment must reorganize to allow for PT to occur.[1] The water molecules that share the proton in both the dihydrate and the trihydrate do not accept strong hydrogen bonds and are already "pre-solvated" in the crystal. This in turn allows the proton to rapidly shuttle back and forth, going through the Eigen−Zundel−Eigen mechanism without the need for significant reorganization of the surrounding solvent.

An exciting aspect of our work is that many of the theoretical results or features that we uncovered can be probed using a combination of DINS and SSNMR experiments. The total $n(p)$ from the DINS measurements gives a robust measure of the role of NQE on the total kinetic energy of the systems. Furthermore, the electronic structure of the excess proton, which was quantified through an analysis of the Wannier centers, yields a distinct signature for protons that exhibit the idealized Zundel-like character. This should be of use for future theoretical studies of proton transfer in other systems. By calculating the NMR parameters of the protons in the acid hydrates we demonstrated that SSNMR is a powerful tool for both determining the strength of hydrogen bonds and probing the dominant limiting state of the proton. We also highlighted the influence of finite temperature effects and NQE on the different ^{1}H SSNMR spectra. Our theoretical studies provide the motivation for new experiments on the hydrogen chloride hydrates which should be facilitated by recent methodological advancements in NMR.[35]

■ ASSOCIATED CONTENT

Ⓢ Supporting Information

Benchmarks that compare radial distributions of the monohydrate using QT and the PI+GLE methodology as well as some more details regarding the differences between the two approaches; details of simulation times for each acid hydrate, radial distributions for the monohydrate, and proton momentum distributions for the dihydrate; discussion on the issues behind the spurious structures obtained from the small unit cells of the mono- and dihydrate; and discussion about the calculated anisotropy and asymmetry of the NMR tensors. This material is available free of charge via the Internet at http://pubs.acs.org.

■ AUTHOR INFORMATION

Corresponding Author

ali.hassanali@phys.chem.ethz.ch; cuny.jerome@phys.chem.ethz.ch

Author Contributions

‡A.A.H. and J.C. contributed equally to this work.

Notes

The authors declare no competing financial interest.

■ ACKNOWLEDGMENTS

This manuscript is dedicated to the late Victoria Buch for her significant contribution to understanding protonated systems. The Swiss National Supercomputing Center (CSCS) and High Performance Computing Group of ETH Zurich are thanked for computational resources. Financial support from the European Union grant (ERC-2009-AdG-247075) from the Royal Society and the Swiss National Science Foundation is gratefully acknowledged. The authors acknowledge Gareth Tribello and Federico Giberti for a critical reading of the manuscript. The authors also thank Alessandro Curioni, Teodoro Laino, and Marcella Ianuzzi for assistance with the CPMD and Quantum ESPRESSO calculations.

■ REFERENCES

(1) Marx, D.; Chandra, A.; Tuckerman, M. E. *Chem. Rev.* **2010**, *110*, 2174−2216.
(2) Cox, J. M.; Timmer, R. L. A.; Bakker, H. J.; Park, S.; Agmon, N. *J. Phys. Chem. A* **2009**, *113*, 6599−6606.
(3) Rini, M.; Magnes, B.-Z.; Pines, E.; Nibbering, E. T. J. *Science* **2003**, *301*, 349−352.
(4) Fang, C.; Frontiera, R. R.; Tran, R.; Mathies, R. A. *Nature* **2009**, *462*, 200−204.
(5) Tuckerman, M.; Laasonen, K.; Sprik, M.; Parrinello, M. *J. Phys. Chem.* **1995**, *99*, 5749−5752.
(6) Tuckerman, M.; Laasonen, K.; Sprik, M.; Parrinello, M. *J. Chem. Phys.* **1995**, *103*, 150−161.
(7) Agmon, N. *Chem. Phys. Lett.* **1995**, *244*, 456−462.
(8) Hynes, J. T. *Nature* **1999**, *397*, 565−567.
(9) Geissler, P. L.; Dellago, C.; Chandler, D.; Hutter, J.; Parrinello, M. *Science* **2001**, *291*, 2121.
(10) Hassanali, A.; Prakash, M. K.; Eshet, H.; Parrinello, M. *Proc. Natl. Acad. Sci. U.S.A.* **2011**, *108*, 20410−20415.
(11) Knight, C.; Voth, G. A. *Acc. Chem. Res.* **2012**, *45*, 101−109.
(12) Eigen, M. *Angew. Chem., Int. Ed. Engl.* **1964**, *3*, 1−19.
(13) Zundel, G.; Metzger, H. *Z. Phys. Chem.* **1968**, *58*, 225−245.
(14) Marx, D. *ChemPhysChem* **2007**, *8*, 209−210.
(15) Markovitch, O.; Chen, H.; Izvekov, S.; Paesani, F.; Voth, G. A; Agmon, N. *J. Phys. Chem. B* **2008**, *112*, 9456−9466.
(16) Berkelbach, T. C.; Lee, H.-S.; Tuckerman, M. E. *Phys. Rev. Lett.* **2009**, *103*, 238302.

(17) Tuckerman, M. E.; Marx, D.; Klein, M. L.; Parrinello, M. *Science* **1997**, *275*, 817.
(18) Marx, D.; Tuckerman, M. E.; Hutter, J.; Parrinello, M. *Nature* **1999**, *397*, 601−604.
(19) Marx, D.; Tuckerman, M. E.; Parrinello, M. *Nature* **2002**, *417*, 925−929.
(20) Benoit, M.; Marx, D.; Parrinello, M. *Nature* **1998**, *392*, 258−261.
(21) Benoit, M.; Marx, D. *ChemPhysChem* **2005**, *6*, 1738−1741.
(22) Voth, G. A. *Acc. Chem. Res.* **2006**, *39*, 143−150.
(23) Walker, M.; Pulham, C. R.; Morrison, C. A.; Allan, D. R.; Marshall, W. G. *Phys. Rev. B: Condens. Matter Mater. Phys.* **2006**, *73*, 224110.
(24) Buch, V.; Dubrovskiy, A.; Mohamed, F.; Parrinello, M.; Sadlej, J.; Hammerich, A. D.; Devlin, J. P. *J. Phys. Chem. A* **2008**, *112*, 2144−2161.
(25) Buch, V.; Mohamed, F.; Parrinello, M.; Devlin, J. P. *J. Chem. Phys.* **2007**, *126*, 074503.
(26) Yoon, Y. K.; Carpenter, G. B. *Acta Crystallogr.* **1959**, *12*, 17−20.
(27) Lundgren, J.-O.; Olovsson, I. *Acta Crystallogr.* **1967**, *23*, 966−971.
(28) Lundgren, J.-O.; Olovsson, I. *Acta Crystallogr.* **1967**, *23*, 971−976.
(29) Taesler, I.; Lundgren, J.-O. *Acta Crystallogr. B* **1978**, *34*, 2424−2428.
(30) Hayes, R. L.; Paddison, S. J.; Tuckerman, M. E. *J. Phys. Chem. B* **2009**, *113*, 16574−16589.
(31) Hayes, R. L.; Paddison, S. J.; Tuckerman, M. E. *J. Phys. Chem. A* **2011**, *115*, 6112−6124.
(32) Ceriotti, M.; Bussi, G.; Parrinello, M. *J. Chem. Theor. Comput.* **2010**, *6*, 1170−1180.
(33) Andreani, C.; Colognesi, D.; Mayers, J.; Reiter, G. F.; Senesi, R. *Adv. Phys.* **2005**, *54*, 377−469.
(34) MacKenzie, K. J. D.; Smith, M. E. *Multinuclear Solid-state NMR of Inorganic Materials*; Pergamon: New York, 2002.
(35) Harris, R. K.; Wasylishen, R. E.; , Duer, M. J. *NMR Crystallography*; Wiley-VCH: New York, 2009.
(36) Abbatt, J. P. D; Beyer, K. D.; Fucaloro, A. F.; McMahon, J. R.; Wooldridge, P. J.; Zhang, R.; Molina, M. J. *J. Geophys. Res.* **1992**, *97*, 15819−15826.
(37) Ayotte, P.; Marchand, P.; Daschbach, J. L.; Smith, R. S.; Kay, B. D. *J. Phys. Chem. A* **2011**, *115*, 6002−6014.
(38) Rosenvinge, T. v.; Tuckerman, M. E. ; Klein, M. L. *Faraday Discuss.* **1997**, *106*, 273−289.
(39) VandeVondele, J.; Krack, M.; Mohamed, F.; Parrinello, M.; Chassaing, T.; Hutter, J. *Comput. Phys. Commun.* **2005**, *167*, 103−128.
(40) Car, R.; Parrinello, M. *Phys. Rev. Lett.* **1985**, *55*, 2471.
(41) Goedecker, S.; Teter, M.; Hutter, J. *Phys. Rev. B: Condens. Matter Mater. Phys.* **1996**, *54*, 1703−1710.
(42) Becke, A. D. *Phys. Rev. A: At., Mol., Opt. Phys.* **1988**, *38*, 3098−3100.
(43) Lee, C.; Yang, W.; Parr, R. G. *Phys. Rev. B: Condens. Matter Mater. Phys.* **1988**, *37*, 785−789.
(44) Ceriotti, M.; Miceli, G.; Pietropaolo, A.; Colognesi, D.; Nale, A.; Catti, M.; Bernasconi, M.; Parrinello, M. *Phys. Rev. B: Condens. Matter Mater. Phys.* **2010**, *82*, 174306.
(45) Ceriotti, M.; Manolopoulos, D. E.; Parrinello, M. *J. Chem. Phys.* **2011**, *134*, 084104.
(46) Morrone, J. A.; Srinivasan, V.; Sebastiani, D.; Car, R. *J. Chem. Phys.* **2007**, *126*, 234504.
(47) Segall, M. D.; Lindan, P. J. D.; Probert, M. J.; Pickard, C. J.; Hasnip, P. J.; Clark, S. J.; Payne, M. C. *J. Phys.: Condens. Matter* **2002**, *14*, 2717−2744.
(48) Pickard, C. J.; Mauri, F. *Phys. Rev. B: Condens. Matter Mater. Phys.* **2001**, *63*, 245101.
(49) Yates, J. R.; Pickard, C. J.; Mauri, F. *Phys. Rev. B: Condens. Matter Mater. Phys.* **2007**, *76*, 024401.
(50) Thibault, C. *Solid State Nucl. Magn. Reson.* **2011**, *40*, 1−20.
(51) Haeberlen, U.. *High resolution NMR in solids. Selective averaging*; Academic Press: New York, 1976.
(52) Monkhorst, H. J.; Pack, J. D. *Phys. Rev. B: Condens. Matter Mater. Phys.* **1976**, *13*, 5188−5192.
(53) Dumez, J.-N.; Pickard, C. J. *J. Chem. Phys.* **2009**, *130*, 104701−8.
(54) Robinson, M.; Haynes, Peter D. *J. Chem. Phys.* **2010**, *133*, 084109−9.
(55) De Gortari, I.; Portella, G.; Salvatella, X.; Bajaj, V. S.; van der Wel, P. C. A.; Yates, J. R.; Segall, M. D.; Pickard, C. J.; Payne, M. C.; Vendruscolo, M. *J. Am. Chem. Soc.* **2010**, *132*, 5993−6000.
(56) Kittel, C.. *Introduction to Solid State Physics*; Wiley-VCH: New York, 1996.
(57) The fluxional character of the hydronium ion is characterized by the umbrella-breathing mode as well as transient PT to the Cl^- (which is a rare event but more enhanced in the quantum simulations). Thus, in the analysis of z_u we do not distinguish between the ion-pair states and these PT events.
(58) All histograms in the present work have been computed using a fine grid and a triangular binning function with a width comparable to the bin size that one would have used with a conventional histogram. This allows one to obtain smoother histograms without artificial loss of resolution. We report histograms in terms of the temperature-scaled free energy, which makes more apparent the probability density for finding the system in a given state.
(59) Fulton, J. L.; Balasubramanian, M. *J. Am. Chem. Soc.* **2010**, *132*, 12597−12604.
(60) Walewski, L.; Forbert, H.; Marx, D. *J. Phys. Chem. Lett.* **2011**, *2*, 3069−3074.
(61) VandeVondele, J.; Mohamed, F.; Krack, M.; Hutter, J.; Sprik, M.; Parrinello, M. *J. Chem. Phys.* **2005**, *122*, 014515.
(62) Morrone, J. A.; Car, R. *Phys. Rev. Lett.* **2008**, *101*, 017801.
(63) de la Peña, L. H.; Kusalik, P. G. *J. Am. Chem. Soc.* **2005**, *127*, 5246−5251.
(64) Paesani, F.; Iuchi, S.; Voth, G. A. *J. Chem. Phys.* **2007**, *127*, 074506.
(65) Paesani, F.; Yoo, S.; Bakker, H. J.; Xantheas, S. S. *J. Phys. Chem. Lett.* **2010**, *1*, 2316−2321.
(66) Morrone, J. A.; Lin, L.; Car, R. *J. Chem. Phys.* **2009**, *130*, 204511.
(67) Sillanpää, A.; Laasonen, K. *ChemPhysChem* **2005**, *6*, 1879−1883.
(68) Aherne, D.; Tran, V.; Schwartz, B. J. *J. Phys. Chem. B* **2000**, *104*, 5382−5394.
(69) Luo, H.; Tucker, S. C. *J. Phys. Chem.* **1996**, *100*, 11165−11174.
(70) Maritz, J. S. *Distribution-Free Statistical Methods*; Chapman and Hall: New York, 1981.
(71) Zundel, G. *Adv. Chem. Phys.* **2007**, 1−217.
(72) Silvestrelli, P. L.; Parrinello, M. *Phys. Rev. Lett.* **1999**, *82*, 3308−3311.
(73) Schwegler, E.; Galli, G.; Gygi, F.; Hood, R. Q. *Phys. Rev. Lett.* **2001**, *87*, 265501.
(74) Kaupp, M.; Bühl, M.; Malkin, V. G. *Calculation of NMR and EPR Parameters: Theory and Applications*; Wiley-VCH: New York, 2004.
(75) Mauri, F.; Pfrommer, B. G.; Louie, S. G. *Phys. Rev. Lett.* **1996**, *77*, 5300−5303.
(76) Sebastiani, D.; Parrinello, M. *J. Phys. Chem. A* **2001**, *105*, 1951−1958.
(77) Thonhauser, T.; Ceresoli, D.; Mostofi, A. A.; Marzari, N.; Resta, R.; Vanderbilt, D. *J. Chem. Phys.* **2009**, *131*, 101101−4.
(78) Mauri, F.; Pfrommer, B. G.; Louie, S. G. *Phys. Rev. Lett.* **1997**, *79*, 2340.
(79) Pfrommer, B. G.; Mauri, F.; Louie, S. G. *J. Am. Chem. Soc.* **1999**, *122*, 123−129.
(80) Mauri, F.; Pasquarello, A.; Pfrommer, B. G.; Yoon, Y.-G.; Louie, S. G. *Phys. Rev. B: Condens. Matter Mater. Phys.* **2000**, *62*, R4786−R4789.
(81) Murakhtina, T.; Heuft, J.; Meijer, E. J.; Sebastiani, D. *ChemPhysChem* **2006**, *7*, 2578−2584.
(82) Ludueña, G. A.; Wegner, M.; Bjålie, L.; Sebastiani, D. *ChemPhysChem* **2010**, *11*, 2353−2360.

(83) Wegner, M.; Dudenko, D.; Sebastiani, D.; Palmans, A. R. A.; de Greef, T. F. A.; Graf, R.; Spiess, H. W. *Chem. Sci.* **2011**, *2*, 2040−2049.
(84) Sebastiani, D.; Parrinello, M. *ChemPhysChem* **2002**, *3*, 675−679.
(85) Banyai, D. R.; Murakhtina, T.; Sebastiani, D. *Magn. Reson. Chem.* **2010**, *48*, S56−S60.
(86) Vaara, J.; Lounila, J.; Ruud, K.; Helgaker, T. *J. Chem. Phys.* **1998**, *109*, 8388−8397.
(87) Kita, Y.; Tachikawa, M. *J. Mol. Struct.: THEOCHEM* **2009**, *912*, 2−4.
(88) Limbach, H.-H.; Tolstoy, P. M.; Parez-Hernandez, N.; Guo, J.; Shenderovich, I. G.; Denisov, G. S. *Isr. J. Chem.* **2009**, *49*, 199−216.
(89) Swanson, J. M. J.; Simons, J. *J. Phys. Chem. B* **2009**, *113*, 5149−5161.